American Journal of Fluid Dynamics 2017, 7(1): 12-22
DOI: 10.5923/j.ajfd.20170701.02

Preliminary Study of Supersonic Partially Covered Cavity Flow with Scaled Adaptive Simulation

Christopher Teruna*, Duck Joo Lee

Department of Aerospace Engineering, KAIST, Daejeon, South Korea

Abstract We investigate supersonic flow over rectangular cavities of 3 different length-to-depth ratio (L/D) – 3, 4.5, and 6. Half of the length of the cavities will be covered additional lids of D/d = 6, in which D/d is the ratio of cavity depth to lid thickness. The lids were installed to either leading edge (FP), trailing edge (BP), or both edges (CP) of the cavities, resulting in 12 variety of cavity configurations. Validation study was performed beforehand to ensure the reliability of Scaled Adaptive Simulation (SAS) turbulence model for supersonic cavity flow simulation in 2-dimensional (2D) domain. Subsequently, pressure fluctuation on cavity floor was obtained through numerical simulation on each cavity model and its frequency response was analysed. The use of partial cover was found to shorten the length of shear layer, which in turn caused mode switching in dominant cavity tones and various changes in mean pressure distribution. Furthermore, certain flowfield characteristics of partially covered cavities were also identified, depending on partial cover configuration and cavity length. These characteristics are also similar to those previously observed in subsonic partially covered cavity flow.

Keywords Cavity flow, Scale adaptive simulation, CFX, Frequency response, Pressure distribution

1. Introduction

The study of cavity flow has always been one of the most intriguing topics among fluid dynamics scholars since it involves various physical attributes, such as aerodynamics and acoustics. Early studies, notably by Karamcheti [1] and Rossiter [2] found that high speed flow over cavity would produce self-sustaining pressure fluctuation inside the cavity and sound radiation away from it. The frequency domain of the pressure fluctuation has several discrete peaks that possess most energy in the spectra, and were subsequently referred to as cavity tones.

Rossiter also revealed that cavity tones are products of a feedback mechanism that involved both fluid and acoustic physics that originated from the shear layer spanning across the cavity due to velocity difference between high velocity freestream and stagnant flow inside the cavity. The shear layer, which evolved from upstream boundary layer, is "flapping" upward and downward periodically, and at some point, impinges on the cavity's aft wall (also referred to as trailing edge in Figure 1). This impingement produces acoustic wave that will propagate upstream along the cavity floor. As these waves arrive at the cavity's front wall, they would excite and subsequently produce more instabilities in the newly developed shear layer at the cavity's leading edge. Thus, the system forms a close loop between fluid and acoustic interactions surrounding the cavity.

Rossiter also proposed a method to predict cavity tones with a semi-empirical equation, commonly referred as Rossiter equation, which relates cavity tones to the cavity length (L), freestream velocity (u_∞) and Mach number (M_∞), and a few empirical constants. Rossiter equation applies for transonic flow over "open" cavity, whose length-to-depth ratio (L/D) is less than 10 (Srivastava [3]). Heller et al. [4] expanded the equation for supersonic flow which is written as follows:

$$f_n = \frac{u_\infty}{L} \cdot \frac{n-\alpha}{\frac{1}{k} + \frac{M_\infty}{\sqrt{1+\frac{\gamma-1}{2}M_\infty{}^2}}} \tag{1}$$

The empirical constant k is ratio of shear layer instability convection velocity to freestream velocity, while α is phase delay between the moment of shear layer impingement and acoustic wave generation. (1) was thought to be valid for all ranges of supersonic Mach number, but Unalmis et al. [5] found that Rossiter equation starts to lose its physical implication in hypersonic flow (Mach 5). Rossiter equation modification for partially covered cavities in subsonic and transonic flow has been proposed by Wittich and Jumper [6], but studies on such cavities are still fairly limited, including Heo [7], Syed and Hoffmann [8], and Permachandran et al. [9]. Therefore, present study aims to expand the investigation into supersonic regime while characterizing phenomena inherent to partially covered cavity

* Corresponding author:
christopherteru@kaist.ac.kr (Christopher Teruna)
Published online at http://journal.sapub.org/ajfd

configurations. This work will also attempt to find relation between supersonic and subsonic partially covered cavity flow.

2. Methodologies

2.1. Numerical Setup

Since this numerical study would be a precursor to experimental campaign, the numerical setup will be based on experimental equipment which is briefly discussed here. Experiments will be carried out in ST-15 supersonic wind tunnel of High Speed Laboratory of Delft University of Technology. The chosen freestream flow conditions can be found in table 1. The blow-down wind tunnel is operable within Mach number of 1.5 – 3.0 by using suitable nozzle and adjusting total pressure (P_o). Total temperature (T_o) depends on air temperature in pressurized air tank that is placed outdoor and thus variations are affected by daily outdoor air temperature. Therefore, small variations in operating condition might exist but were neglected in numerical simulation.

Table 1. Freestream conditions used for present work

M_∞	P_o	T_o	Re_L of L/D=6
3	4.7 bar	285 K	4.8 million

Re_L is defined as Reynolds number of cavity length.

Table 2. Model nomenclature in present work

Model	*L/D*	Lid length (*l*)	Cover Type	Illustration
B3	3			
B45	4.5	None	None	
B6	6			
B3BP	3			
B45BP	4.5	0.5*L*	Back plate	
B6BP	6			
B3CP	3			
B45CP	4.5	0.25*L*×2	Front and Back plate	
B6CP	6			
B3FP	3			
B45FP	4.5	0.5*L*	Front plate	
B6FP	6			

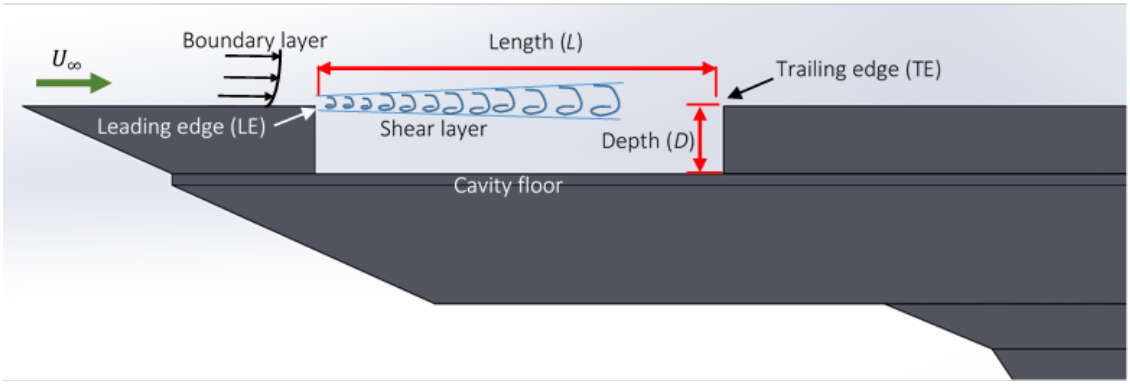

Figure 1. Nomenclature of cavity flow in this paper

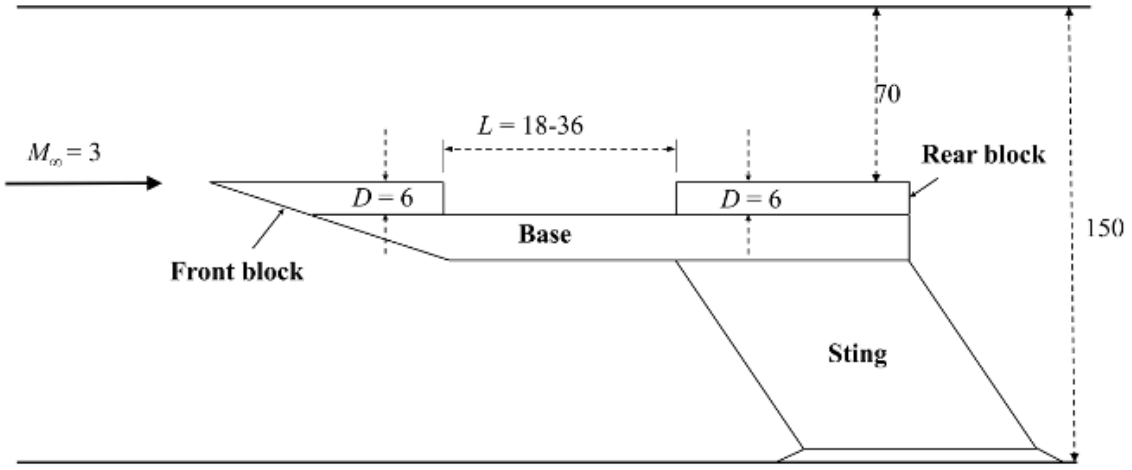

Figure 2. Side view of cavity model used in present study, dimensions are given in millimetres (mm)

The computational domain is constructed based on actual model that will be manufactured for experimental campaign. As shown in Figure 2, the length of the cavity could be set between 18 mm (L/D = 3) and 36 mm (L/D = 6). The model width (W) is 120 mm in order to obtain $L/W < 1$ according to 2-dimensional cavity requirement given by Ahuja and Mendoza [10]. This would allow 2D computational domain to be used to reduce computational load, although validation study will also be performed to confirm this. Moreover, vertical distance between the cavity and the ceiling was adjusted as 70 mm so that any shockwave that is radiated from within the cavity will not be reflected by the upper wall back into the model.

There are 12 models used in present work. These are specified in Table 2. The additional covers/lids for partially covered cavities were modelled as cavity leading edge or trailing edge extension with 1 mm thickness.

The numerical analysis was performed under the framework of commercial software ANSYS CFX that supports SAS turbulence model. Meanwhile, domain meshing was carried out with ICEM CFD using multi-block structured grid generation. The 2-dimensional computational domain and its parameters are given in Figure 3 and Table 3 respectively.

Table 3. Computational domain setup parameters

Edge	Length	# of cells
L_0	5 mm	15
L_1	25.8 mm	60
L	18 mm (L/D=3)	152 (L/D=3)
	27 mm (L/D=4.5)	177 (L/D=4.5)
	36 mm (L/D=6)	202 (L/D=6)
L_2	101.2 mm (L/D=3)	150 (L/D=3)
	92.2 mm (L/D=4.5)	125 (L/D=4.5)
	83.2 mm (L/D=6)	100 (L/D=6)
D	6 mm	64
H	70 mm	100

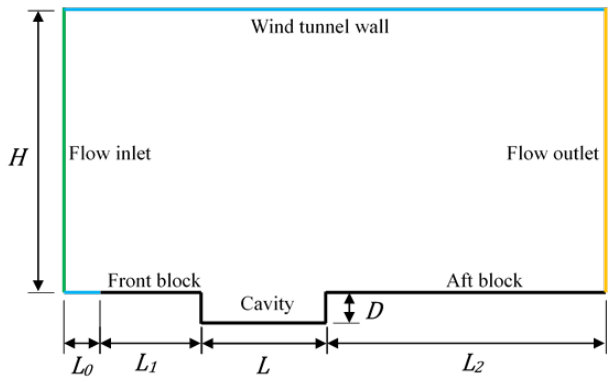

Figure 3. 2-D computational domain for present study

To simplify the simulation, only upper half of the wind tunnel test section was modelled, which is similar to previous ANSYS FLUENT simulation by Sridhar et. al. [11]. Grid parameters for present work were also specified similarly. Mesh bunching was applied at near-wall and shear layer regions with hyperbolic law, resulting in approximately 50,000 mesh cells in total. Near-wall grid spacing (y^+) was specified to be less than 8 and grid expansion ratio was set to be 1.2 throughout the domain. Samples of the 2D domains are shown in Figure 4. Inlet boundary condition is specified as supersonic inlet with u_∞ = 606 m/s, with total pressure and total temperature as prescribed in Table 1. The domain extension upstream of front block is defined as free-slip wall to ensure uniform flow parallel to the front block surface. No-slip wall boundary condition is applied to wind tunnel and cavity model walls, while non-reflecting boundary condition is imposed at the outlet.

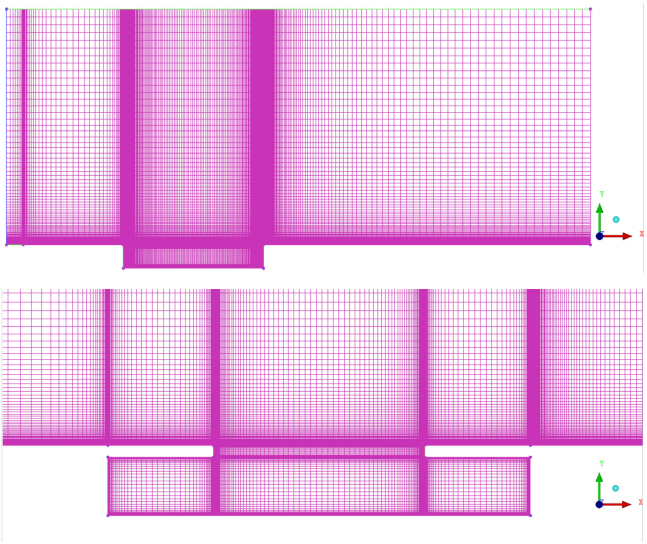

Figure 4. Mesh generated with ICEM CFD: whole domain of B6 (above) and a close up mesh near B6CP cavity (below)

Temporal discretization is based on second-order backward Euler while second-order high-resolution scheme is applied for advection and diffusion term. The same high-resolution scheme is used to compute Scaled Adaptive Simulation (SAS) turbulence model computation. The simulation was performed with time stepping of 2 μs for 60,000 iterations in order to resolve frequency of interest of around 15 kHz by roughly 20 points.

2.2. Scaled Adaptive Simulation

This section will briefly introduce SAS-SST turbulence model that is applied in ANSYS CFX. More in-depth details of SAS and its implementation in CFX can be found in [12], [13], and [14].

SAS is an improvement over conventional k-ω model – which is a RANS model, by introducing von Karman length scale in the turbulence scale equation. This allows SAS to adapt resolved turbulent spectrum according to unsteadiness in the flowfield. Practically, SAS is applied as additional source term Q_{SAS} in turbulence dissipation equation, ω. To elaborate, k-ω-SST equations with Q_{SAS} in ANSYS CFX are given as follows:

$$\frac{\partial(\rho k)}{\partial t}+\frac{\partial(\rho U_i k)}{\partial x_i}=-\frac{\partial}{\partial x_i}\left[\frac{\partial k}{\partial x_i}\left(\mu+\frac{\mu_t}{\sigma_k}\right)\right]-\beta_k\rho k\omega+P_k$$

$$\frac{\partial(\rho\omega)}{\partial t}+\frac{\partial(\rho U_i\omega)}{\partial x_i}=-\frac{\partial}{\partial x_i}\left[\frac{\partial\omega}{\partial x_i}\left(\mu+\frac{\mu_t}{\sigma_\omega}\right)\right]-\beta_\omega\rho\omega^2+\alpha\frac{k}{\omega}P_k$$
$$+(1-F_1)\frac{2\rho}{\omega\sigma_{\omega 2}}\frac{\partial k}{\partial x_i}\frac{\partial\omega}{\partial x_i}+Q_{SAS} \quad (2)$$

Q_{SAS} is defined as follows:

$$Q_{SAS}=\max\left[\rho\zeta_2 kS^2\left(\frac{L}{L_{vK}}\right)^2-C\frac{2k}{\sigma_\varphi}\max\left(\frac{1}{\omega^2}\frac{\partial\omega}{\partial x_i}\frac{\partial\omega}{\partial x_j},\frac{1}{k^2}\frac{\partial k}{\partial x_i}\frac{\partial k}{\partial x_j}\right),0\right] \quad (3)$$

Some parameters in (3) include $\zeta_2=3.51$, $\sigma_\varphi=2/3$, and C = 2. Meanwhile, L is the length scale of modelled turbulence, L_{vK} is von Karman length scale, which is generalized from its boundary layer definition, and S is scalar invariant of strain rate tensor S_{ij}.

$$L=\frac{\sqrt{k}}{c_\mu^{0.25}\omega},\quad c_\mu=0.09 \quad (4)$$

$$L_{vK}=\frac{kS}{\sqrt{\sum\left(\frac{\partial^2 U_i}{\partial x_i\partial x_j}\right)^2}} \quad (5)$$

$$S=\sqrt{2S_{ij}S_{ij}},\quad S_{ij}=\frac{1}{2}\left[\frac{\partial U_i}{\partial x_j}\frac{\partial U_j}{\partial x_i}\right] \quad (6)$$

In unsteady flowfield, such as shear layer, the term Q_{SAS} will activate due to the term containing von Karman length scale dominating in (3). Nevertheless, Q_{SAS} activation also require local grid size to be small enough to resolve turbulent length scale.

3. CFX 2D Validation Study

While supersonic cavity flowfield is inherently 3-dimensional (3D), it is also interesting to find out if 2-dimensional (2D) simulation would still be adequate (in fact, Rossiter equation is 1-dimensional). After all, parametric analysis for engineering purposes would involve numerous simulations and computing 2D domain would require much lower computational load. However, 2D simulation might produce results with lower accuracy since turbulent flow is inherently 3-dimensional. This validation study will scrutinize the efficacy of 2D-SAS cavity flow simulation.

3.1. Cavity Tones of Mach 2 Supersonic Cavity Flow

This simulation is based on Zhuang's [15] cavity with *L/D* of 5.2 and *L/W* of 5.92 which implies that the cavity is 3-dimensional. Computational domain modelling is similar to Figure 3 except now the cavity is 122 mm long, 23.6 mm deep, and 20.5 mm wide. Inlet flow condition is Mach 2 and u_∞ = 548 m/s.

Frequencies predicted using Rossiter equation, up to mode 6, is plotted in Figure 5 as vertical dashed line with the mode number printed near the horizontal axis. While cavity tone frequencies seemed to be in good agreement, yet there are discrepancies in amplitude, which is defined as sound pressure level (SPL). SPL itself is defined as logarithmic measure of pressure relative to reference value of 20 μPa (threshold of human hearing) in (7).

$$SPL=20\times\log_{10}\left(\frac{p}{20\ \mu\text{Pa}}\right) \quad (7)$$

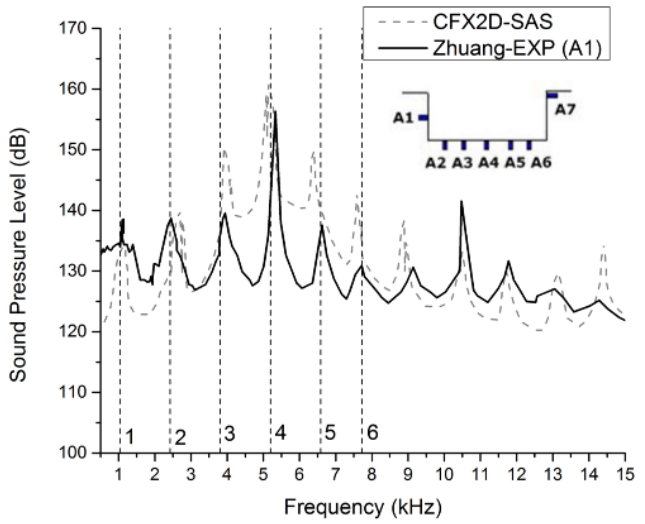

Figure 5. Frequency response of pressure fluctuation at cavity's front wall in Mach 2 supersonic cavity flow

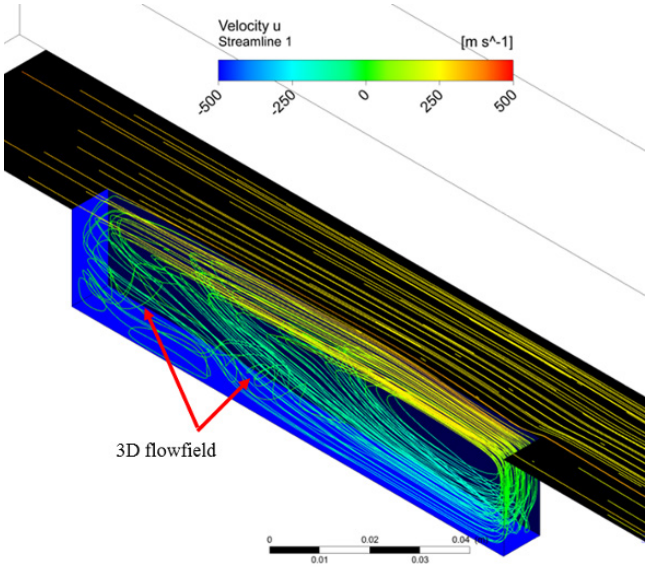

Figure 6. Streamlie of Zhuang's cavity simulation with CFX-SAS. The cavity domain is cut along lengthwise symmetry in this figure

The discrepancies, which are mostly overestimation near the dominant tones, were assumed to originate from

3-dimensional flowfield effects.

To identify the origin of the 3D effect, half-span 3D simulation was performed to investigate mean flowfield over the cavity. The 3D cavity was generated by extruding existing 2D domain in normal direction for additional 40 grids. The result was a 3D domain with 4.5 million elements.

Mean streamline of the cavity is shown in Figure 6, where the wall upstream, downstream, and to the side of the cavities were coloured black. Meanwhile, the cavity's front wall and floor were coloured dark blue. The streamlines inside the shear layer were mostly 2-dimensional and unaffected by the presence of the side wall. However, a few swirling 3D streamlines could be observed (pointed by arrow in Figure 6) at regions near the cavity's leading edge. Although the influence of 3D flowfield is neglected in this study, it is envisaged that 2D simulation of supersonic cavity flow is still reliable to capture frequencies of cavity tones.

3.2. Cavity Floor Pressure Distribution at Mach 3

The second case is a comparison of mean pressure distribution along cavity floor. There are two references for comparison: 1) LES simulation with OpenFOAM by Arya et al. [16] and 2) experimental and *k-ω* simulation results by Gruber et al. [17]. For this case, 2D computational domain was derived from Gruber et al.'s simulation of a cavity with $L/D = 3$ – identical configuration with B3 cavity.

Figure 7 shows that 2D CFX simulation is generally in good agreement with Gruber's experiment, although overestimation is also detected at the upstream region of the cavity. This overestimation could be related to the similar behaviour of frequency response in Figure 5, but at the moment, no conclusive evidence could be found. Nevertheless, present CFX-SAS results seems to be in good agreement with previous experimental and numerical data obtained by others.

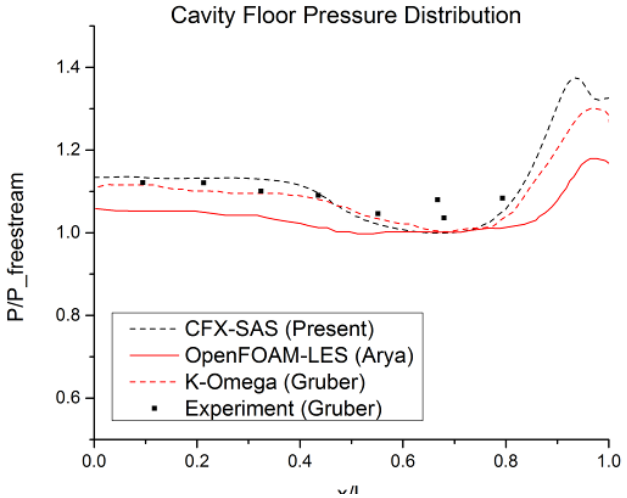

Figure 7. Comparison of mean pressure distribution along cavity floor, vertical axis is defined as ratio of local pressure to freestream pressure

Comparison of Strouhal number of the 1st Rossiter mode between references is given in Table 4. Unfortunately, there was no frequency response from Gruber et. al.'s experiments. Nevertheless, Strouhal number of both present simulation and Arya et. al.'s are relatively close to each other.

Table 4. Comparison of Strouhal number from validation case 2

Reference	*St*, 1st mode	Difference to Mod. Rossiter
Mod. Rossiter (1)	0.232	–
Arya et. al. [16]	0.210	10.7 %
Gruber et. al. [17]	*No data*	
CFX 2D SAS (present)	0.222	4.5 %

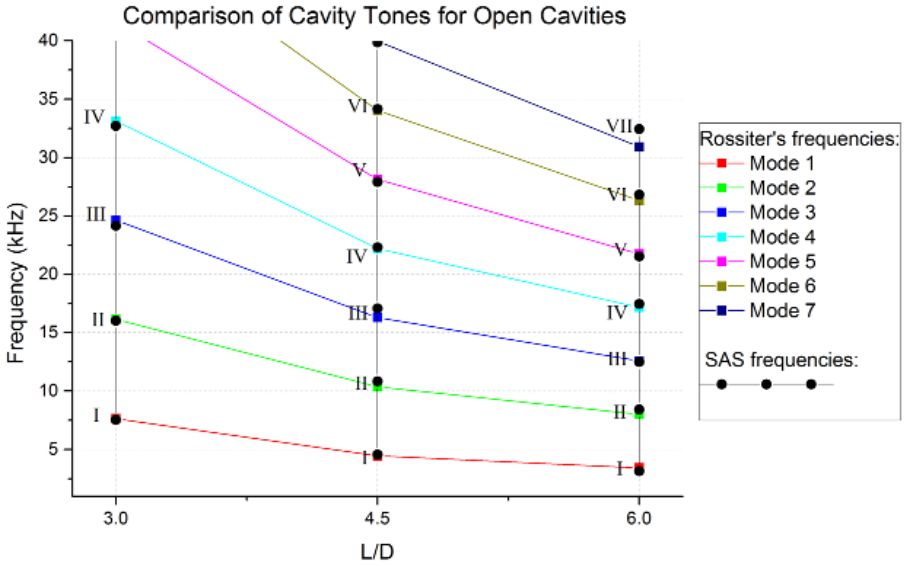

Figure 8. Baseline cavity (B3, B45, and B6) tone frequency comparison to Rossiter equation. Roman numbers correspond to those in Figure 8

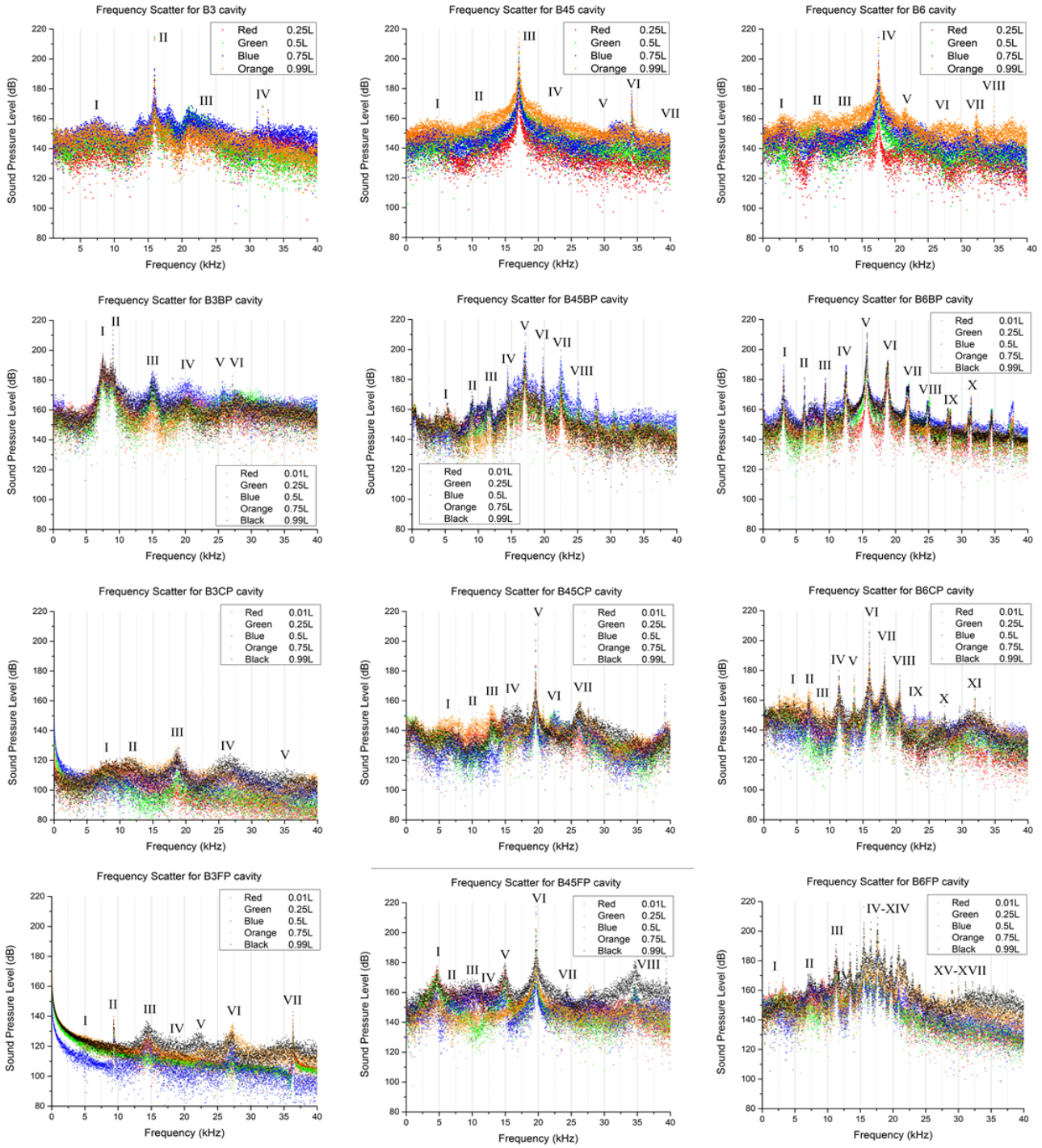

Figure 9. Frequency responses of pressure fluctuation on cavity floor of all cavity models

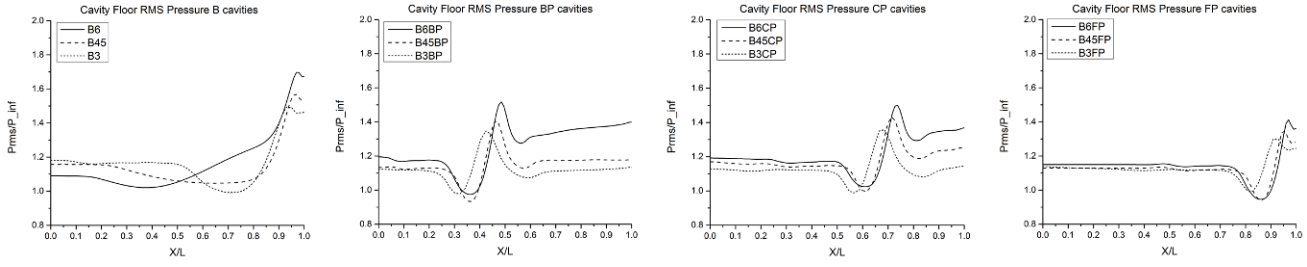

Figure 10. Root-mean-square (RMS) average of pressure distribution along cavity floor, rearranged based on cover/lid configuration. Vertical axis is defined as ratio of local pressure to freestream pressure

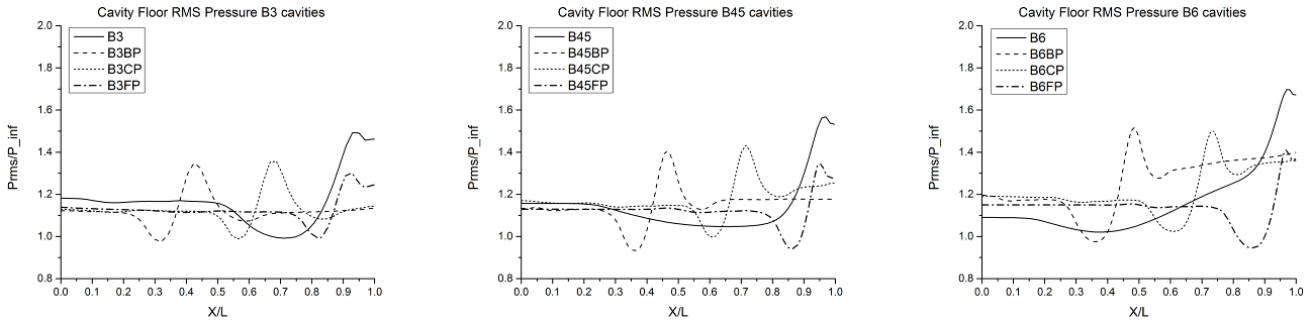

Figure 11. Root-mean-square (RMS) average of pressure distribution along cavity floor, rearranged based on cavity length. Vertical axis is defined as ratio of local pressure to freestream pressure

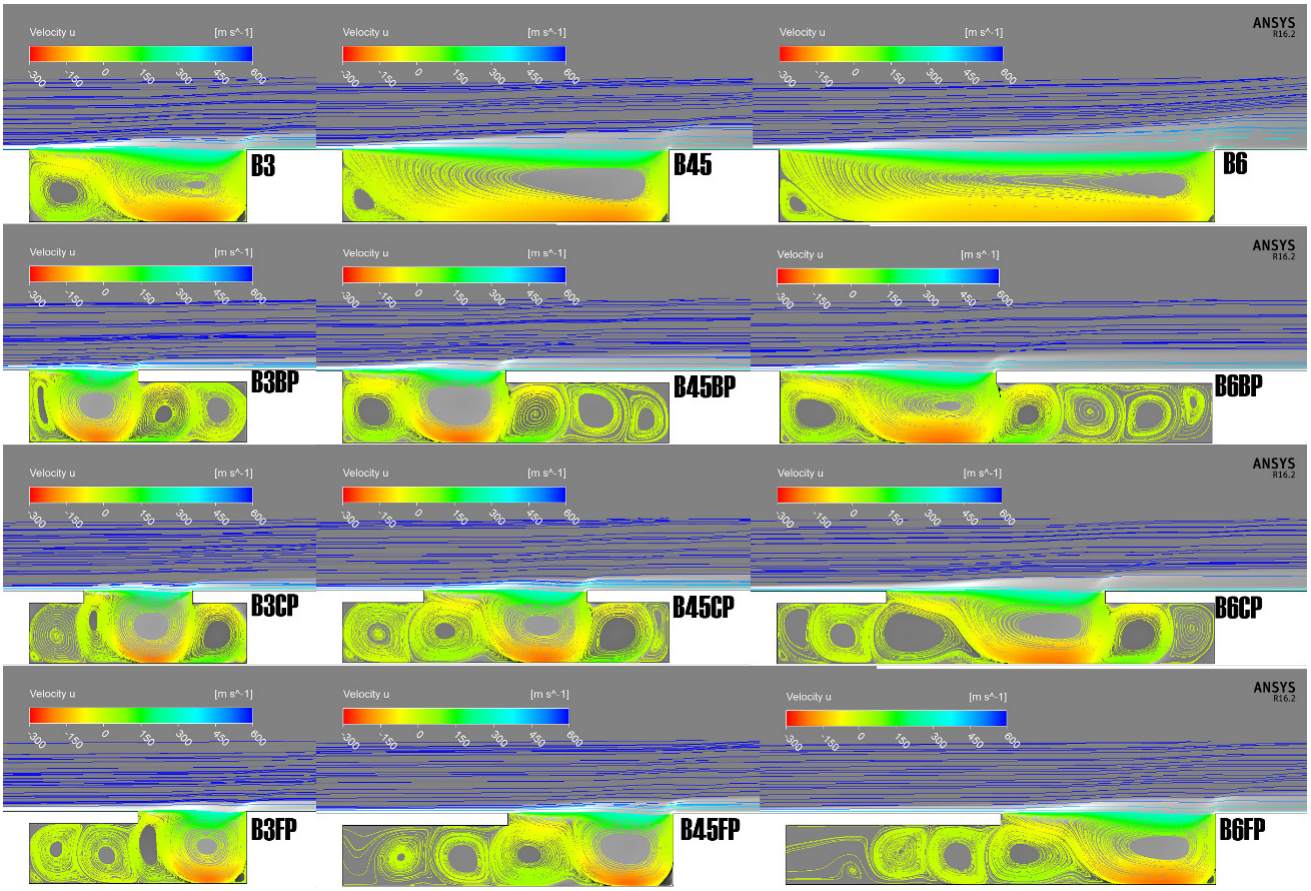

Figure 12. Averaged streamlines and velocity contours

4. Results and Discussions

4.1. Numerical Results

Frequency domain of pressure fluctuation on cavity floor from CFX simulation is shown in Figure 9 where it is arranged according to each model name. For the case of baseline cavity (B3, B45, and B6), tone frequencies (roman numbers) were found to correspond to Rossiter frequencies (i.e. 17.5 kHz of Rossiter mode IV for B6) that were obtained using (1). Although $k = 0.57$ $\alpha = 0.25$ are used typically, but the values that provided better fit are given in Table 5. Comparison between cavity tones of baseline cavities and those from Rossiter equation is given in Figure 8.

Table 5. Rossiter empirical parameters for baseline cavities

L/D	*k*	*α*
3	0.48	0.1
4.5	0.52	0.25
6	0.56	0.25

Figure 9 presents the frequency responses of the 12 cavity models. Roman numbers in Figure 8 is also showed in Figure 9 to label cavity tones. Note that roman numbering for partially covered cavity tones do not correspond to frequencies that are calculated with (1).

Compared to baseline cavities, partially covered models have more number of tones, similar to observations of CP

cavity in subsonic flow by Syed and Hoffmann [8]. Such frequency response would correspond to higher pressure fluctuation, especially at area close to the shear layer impingement location. Nevertheless, unique for the case of B3CP and B3FP, the frequency responses are significantly weaker compared to other models although there are some tones to be identified.

Frequency responses of partially covered cavities are also significantly different from their baseline counterparts. One particular nature of partially covered cavity is mode switching of dominant cavity tones which Heo [7] have previously observed that in subsonic flow. For instance, the dominant tone (highest peak in frequency domain) of B6 is located at 17.5 kHz (mode IV), but in B6BP, B6CP, and B6FP, the dominant tones (mode V, VI, and IV respectively) are closer to 15.5 kHz (mode II) which is the dominant frequency of B3 cavity. Similarly for B45BP, B45CP, and B45FP, the dominant frequency switches from 16.7 kHz to 20 kHz which corresponds to mode II of cavity with L/D=2.25, predicted using Rossiter equation. However, for B3 cavities, this phenomenon is not as clear.

The installation of lid/cover does alter pressure distribution on cavity floor, as demonstrated in Figure 10. Generally, FP lid configuration reduces overall pressure distribution, while BP configuration amplifies it, and CP configuration produces something in between. However, dimension of cavity length may have unique influence as well, which is shown in Figure 11. To elaborate, in the case of B6 partially covered cavities, pressure distribution is increased at locations upstream of shear layer impingement location. The effect is less prominent in B45 cavities and it turns out to be slight pressure reduction for B3 cavities. This behaviour may account for lower SPL amplitude in the frequency domain of B3CP and B3FP cavities.

In Figure 11, streamline structures among baseline cavities are observed to be similar – a large recirculation region (abbreviated as RCR) that spans almost the entire length of the cavity and a smaller one at the lower left corner (Gruber et. al. [17] also obtained similar result in their k-ω simulation). However, when the shear layer becomes shorter due to partial cover, the pair of RCRs below the shear layer would mimic that of baseline cavity with the same shear layer length. For example, the RCRs underneath uncovered area in B6BP, B6CP, and B6FP cavities are strikingly similar to those of B3 cavity. Nevertheless, whether this behaviour is related to the mode switching is yet to be known.

Figure 13 shows that the flowfield inside the cavity is mostly subsonic although reverse flow in certain area may reach as high as Mach 0.6. Velocity field underneath the lid, on the other hand, is mostly dormant as shown in Figure 14, except for regions close to the lid edge where recirculation may reach up to Mach 0.3. These observations imply that the uncovered area mostly influences feedback mechanism (acoustic – fluid mechanics coupling) on partially covered cavities; the covered area would only affect acoustic propagation that could be considered similar to sound waves in a pipe, for example.

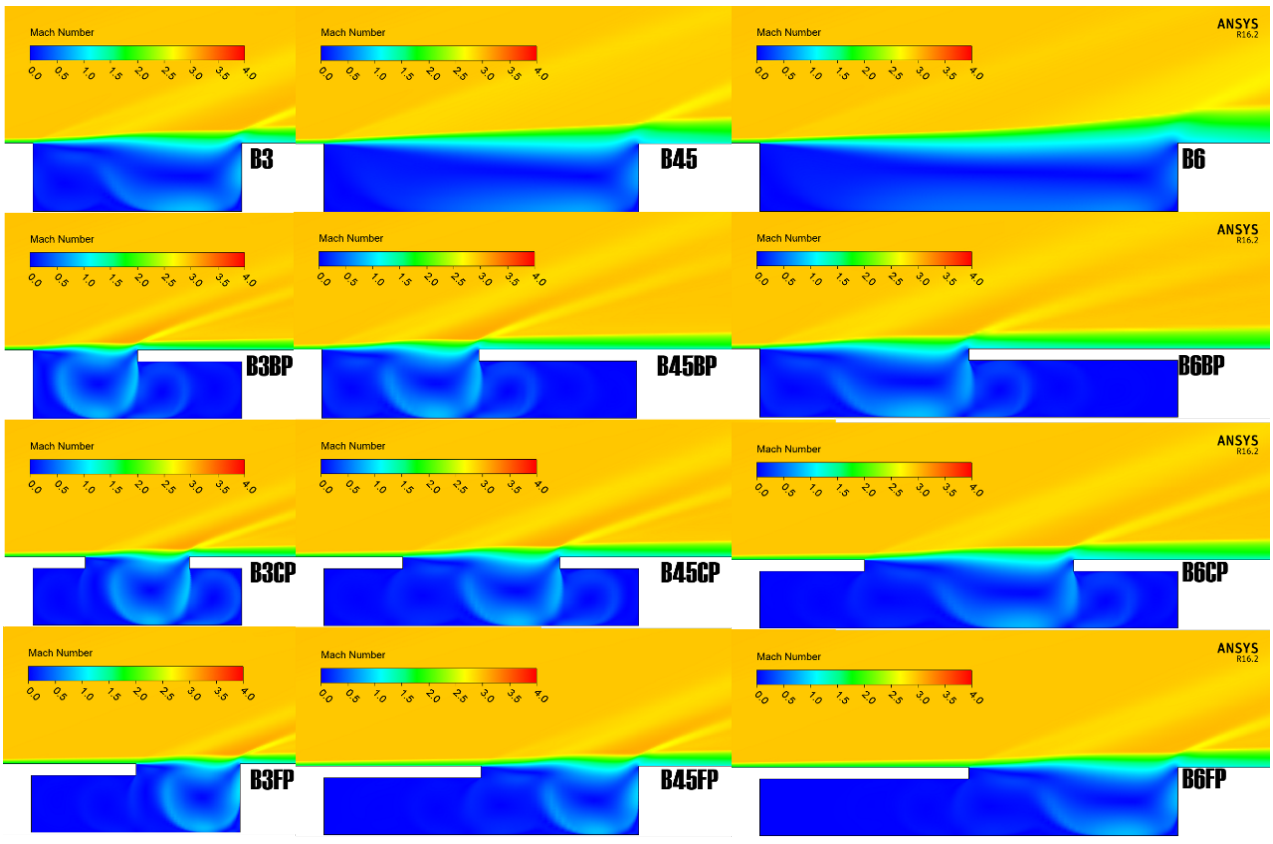

Figure 13. Averaged Mach number contours

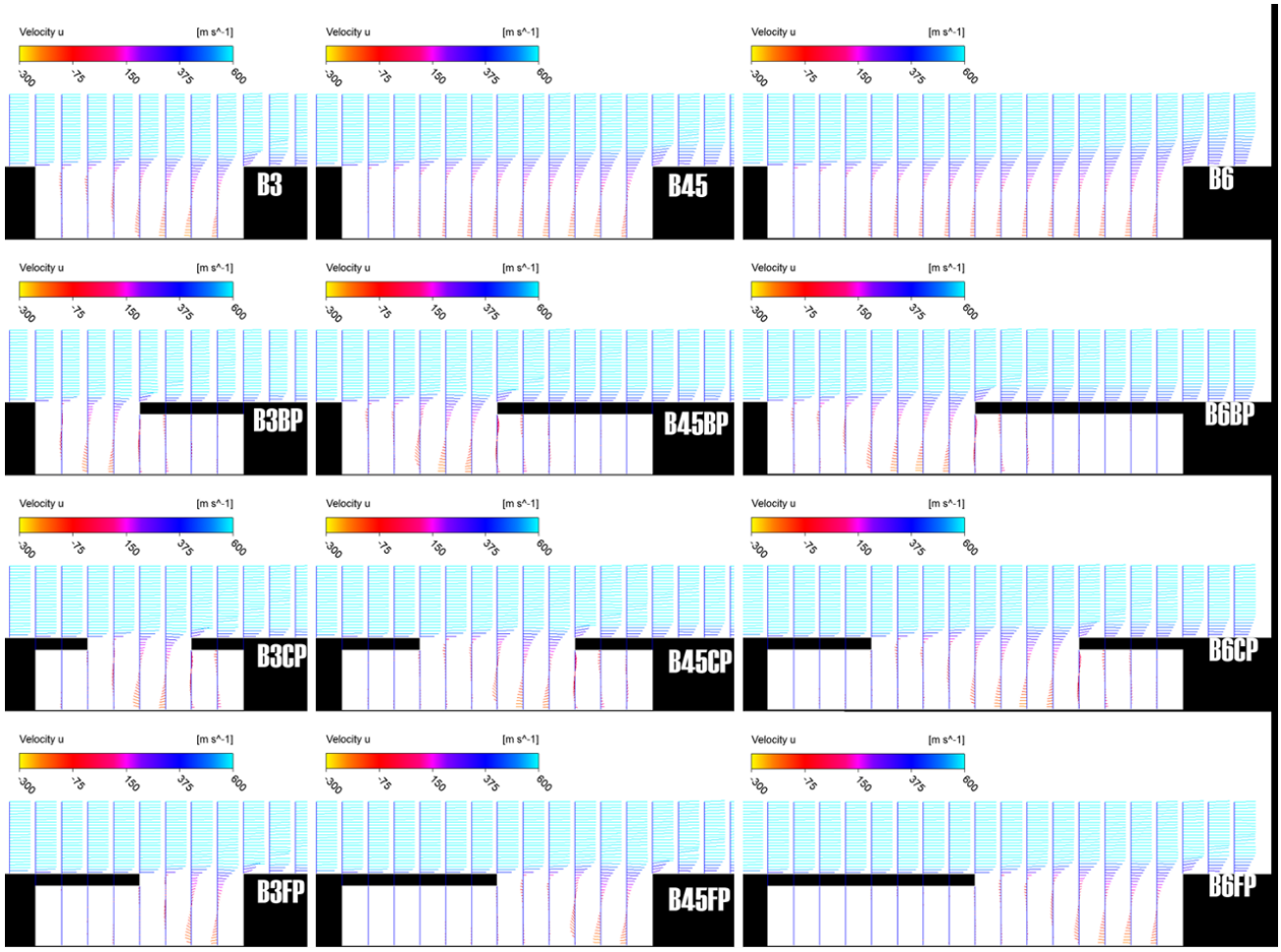

Figure 14. Averaged velocity vector contours

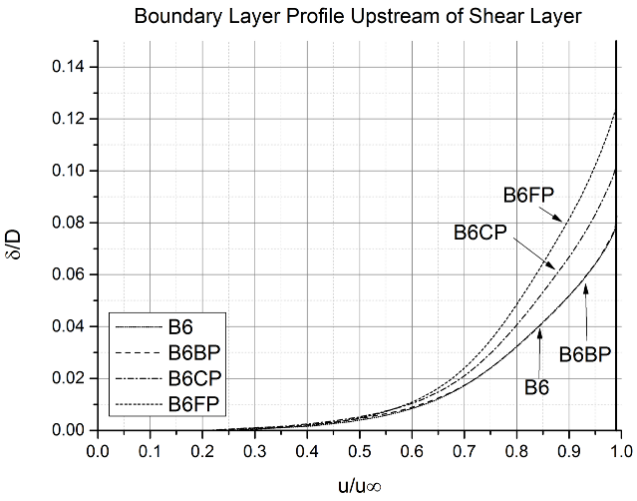

Figure 15. Comparison of velocity profile upstream of shear layer separation. Vertical axis is defined as ratio of boundary layer thickness and cavity depth

A further look into Figure 13 also reveals that FP cavities have thicker boundary layer at the edge of lid before its separation. The thicker boundary layer could be responsible for weaker surface pressure distribution and diffusive frequency response of FP cavities, which Li et al. [18] also found in their numerical study. A comparison on boundary layer profile for B6 cavities is given in Figure 15. The thick vertical line marks boundary layer edge at $0.99u_{\infty}$.

4.2. Applications of Partially covered Cavities

Present study of partially covered cavities also beg a very interesting question: which partial cover configuration exhibit the best overall performance? Unfortunately, there is no definitive or exact answer to it, since the term "best performance" here could vary from different perspectives.

Based on acoustic performance, i.e. lower pressure fluctuation, either CP or FP configuration would be preferable as both reduce overall SPL level compared to BP and baseline configurations. FP cavity in subsonic flow, in fact, has been widely applied for nose landing gear bay and door mechanism [9]. CP configuration is also applicable for landing gear door, since it resembles that of Helmholtz resonator, i.e. muffler, which was found to reduce noise of certain range of frequency.

Meanwhile, BP cavities may be beneficial for high-speed combustion systems, such as ramjet flame-holder. When designing such systems, flow instabilities produced by cavities would enhance fuel-air mixing process. In the case of BP configuration, RCRs inside the cavity were found to be

more energetic, i.e. higher flow velocity underneath the cover, compared to other configurations. Therefore, BP cavity may offer an improvement in flame-holding capability of present cavity-based combustors.

Overall, each cavity configuration possesses different characteristics that would be favourable for different purposes. However, present study did not account for aero-elastic response of the partial cover, which could have a significant influence to the performance of each cavity configuration. Therefore, future investigations into the application of partially covered cavity are still intriguing nonetheless.

5. Conclusions and Outlooks

This paper presents a preliminary study of supersonic flow over various partially covered cavities using Scaled Adaptive Simulation (SAS) in ANSYS CFX which was developed by Egorov and Menter [12, 13]. At first, validation study was performed to assess the efficacy of SAS turbulence model for supersonic cavity flow. The study showed good agreement for pressure distribution on cavity floor; although there was overestimation in sound pressure level (SPL) of frequency response. Similarly, Das and Kurian [19], Hamed et. al. [20] and Nayyar et. al. [21] found that pressure oscillation from 2D simulations of cavity whose $L/W > 1$ would overestimate experimental results while cavity tone frequencies were still resolved within reasonable accuracy.

Subsequently, SAS turbulence model was applied for the simulations of 12 cavity configurations. Baseline cavity tones from SAS were in good agreement with frequencies from Rossiter equation. Frequency responses of partially covered cavities were significantly different to those of baseline cavities. However, certain behaviours such as mode switching of dominant cavity tones were observed. Thus, it is surmised that supersonic partially covered cavity flow is sharing some physical similarities with its subsonic counterpart.

Undoubtedly, doors for future studies are still wide open, especially since present work only accounts for a few variable parameters. Future parametric studies, by accounting variation of d/D, l/L or the geometry of the lid itself, will be required to formulate prediction models of arbitrary partially covered cavities. It is also envisaged that high-accuracy scheme is required to fully resolve acoustic field inside the partially covered cavity that has been overlooked in present work.

ACKNOWLEDGEMENTS

This study is a part of an ongoing research collaboration between KAIST (South Korea) and Delft University of Technology (The Netherlands). The author would like to acknowledge both universities for providing grant and support for computational facilities.

REFERENCES

[1] K. Krishnamurty, “Sound Radiation from Surface Cutouts in High Speed Flow”, PhD. Dissertation, California Institute of Technology, Pasadena, California, USA, 1956.

[2] J. E. Rossiter, “Wind Tunnel Experiments on the Flow over Rectangular Cavities at Subsonic and Transonic Speeds,” Reports and Memoranda No.3438, Ministry of Aviation, UK, Oct. 1966.

[3] A. Srivastava, Application of Machine Learning Techniques for Classification of Cavity Flow and Resonance, Journal of Aircraft, vol. 51(5), pp. 1642–1647, Sep. 2014.

[4] H. H. Heller, G. Holmes, E. E. Covert “Flow-Induced Pressure Oscillations in Shallow Cavities,” Technical Report AFFDL-TR-70-104, Air Force Flight Dynamics Laboratory, Wright-Patterson Air Force Base, Ohio, USA, Dec. 1966.

[5] O. H. Unalmis, N. T. Clemens, D. S. Dolling, Cavity Oscillation Mechanisms in High-Speed Flows, AIAA Journal, vol. 42(10), pp. 2035–2041, Oct. 2004.

[6] D. J. Wittich, E. J. Jumper, Pressure Oscillations Resulting from Subsonic Flow over a Partially Covered Cavity, 41st Plasmadynamics and Lasers Conference, Chicago, Illinois, USA, Jun. 2010.

[7] D. N. Heo, An Identification and Control of the Feedback Mechanism of the Flow and Acoustic Field, PhD. Dissertation, Korea Advanced Institute of Science and Technology, Daejeon, South Korea, 2004.

[8] S. A. Syed, K. A. Hoffmann, Numerical Investigation of 3-D Open Cavity with & without Cover Plates, 47th AIAA Aerospace Sciences Meeting, Orlando, Florida, USA, Jan. 2009.

[9] S. Premachandran, Z. Hu, and X. Zhang, Computational Analysis of Partially covered Cavity with and without Side Walls, 8th AIAA Flow Control Conference, Washington D. C., USA, Jun. 2016.

[10] K. K. Ahuja and J. Mendoza, Effects of Cavity Dimensions, Boundary Layer, and Temperature on Cavity Noise with Emphasis on Benchmark Data to Validate Computational Aeroacoustic Codes, NASA Contractor Report 4653, USA, Apr. 1995.

[11] V. Sridhar, S. L. Gai, and H. Kleine, A Numerical Investigation of Supersonic Cavity Flow At Mach 2, 18th Australasian Fluid Mechanics Conference, Launceston, Australia, Dec. 2012.

[12] F. R. Menter, and Y. Egorov, A Scale-Adaptive Simulation Model using Two-Equation Models, 43rd AIAA Aerospace Sciences Meeting, AIAA 2005-1095, Reno, Nevada, USA, Jan. 2005.

[13] Y. Egorov, and F. R. Menter, Development and Application of SST-SAS Turbulence Model in the DESIDER Project, Second Symposium of Hybrid RANS-LES Methods, Corfu, Greece, Jun. 2007.

[14] “ANSYS CFX Solver Theory Guide,” ANSYS R16.2, ANSYS Inc., USA, 2015.

[15] N. Zhuang, "Experimental Investigation of Supersonic Cavity Flow and Their Control," PhD. Dissertation, Florida State University, USA, Mar. 2007.

[16] N. Arya, R. K. Soni, and A. De, Investigation of Flow Characteristics in Supersonic Cavity Using LES, American Journal of Fluid Mechanics, vol.5(3A), pp.24-32, 2015.

[17] M. R. Gruber, R. A. Baurle, T. Mathur, K. Y. Hsu, Fundamental Studies of Cavity-Based Flame-holder Concepts for Supersonic Combustors, Journal of Propulsion and Power, vol.17(1), pp.146-153, Jan. 2001.

[18] W. Li, T. Nonomura, and K. Fujii, On the Feedback Mechanism in Supersonic Cavity Flows, Physics of Fluids, vol.25, pp.1-15, Jan. 2013.

[19] R. Das and J. Kurian, Acoustic and Velocity Field over 3D Cavities, Theoretical & Applied Mechanics Letters, vol.3, article 012001, Jan. 2013.

[20] A. Hamed, D. Basu, and K. Das, Detached Eddy Simulations Of Supersonic Flow Over Cavity, 41st Aerospace Sciences Meeting and Exhibit, Reno, Nevada, USA, Jan. 2003.

[21] P. Nayyar, G. N. Barakos, and K. J. Badcock, Numerical and Experimental Analysis of Transonic Cavity Flows, International Symposium on Integrating CFD and Experiments in Aerodynamics, Shrivenham, UK, Sep. 2005.